Weierstraß-Institut
für Angewandte Analysis und Stochastik

im Forschungsverbund Berlin e.V.

Pattern formation in intracortical neuronal fields

Axel Hutt[1], Michael Bestehorn[2], Thomas Wennekers[3]

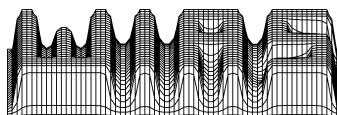submitted: 11th March 2003

[1]   Weierstrass Institute for Applied Analysis and Stochastics,
     Max-Planck-Institute for Mathematics in the Sciences, Leipzig, Germany

[2]   BTU Cottbus, Lehrstuhl für Theoretische Physik II, Cottbus, Germany

[3]   Max-Planck-Institute for Mathematics in the Sciences, Leipzig, Germany

Abstract

The present article introduces a neuronal field model for both excitatory and inhibitory connections. A single integro-differential equation with delay is derived and studied at a critical point by stability analysis, which yields conditions for static periodic patterns and wave instabilities. It turns out that waves only occur below a certain threshold of the activity propagation velocity. An additional brief study exhibits increasing phase velocities of waves with decreasing slope subject to increasing activity propagation velocities, which are in accordance to experimental results. Numerical studies near and far from instability onset supplement the work.

1   Introduction

Measured brain activity by means of encephalography is supposed to originate from collective neuronal behavior [1]. Current source density studies indicate that in some cortical layers, neurons are oriented in a special way to generate a large net activity measured as encephalograms (see [2] and references therein). Suitable basic models for a coherent activity are networks of single coupled neurons on one side and continuous neuronal fields in space on the other. Both approaches have been studied in numerous works (see e.g. [3, 4, 5, 6] and references therein) with different interests. A major aspect of modeling neuronal activity is the examined interaction range of neural excitation and inhibition. It turns out that delay effects occur easily in local interaction models, in contrast to long-range interactions. In recent years, many works have examined delay effects in integrate-and-fire networks [7, 8, 9, 10], spiking neuron networks [11] and pulse coupled networks [12, 13]. However, the study of pattern formation being subject to delay in short-range continuous fields are rare [14].

The present contribution is based on an existing neuronal field model for long-range connections [15, 16, 17, 18]. However, in order to formulate a short-range, i.e. intracortical, field equation, it must be extended in several ways. The model of Jirsa and Haken is formulated as an integral equation with delay and considers one type of neurons, which are connected with other neurons by either excitatory or inhibitory synapses. Long-range connections between neurons are myelinated axonal fibers, which terminate at excitatory synapses, while inhibitory connections are local. This assumption leads to a neglection of effects like lateral inhibition, which are supposed to be important in shaping response properties of cortical cells [19, 20]. As a consequence, the propagation delay along axons represents the only time scale. Our model avoids this constraint and considers both excitatory and inhibitory short-range connections along un-myelinated axonal fibers. From physiology it is known that myelination of axons increases the velocity of propagating pulses. Therefore, intracortical connections reveal lower propagation velocities and, hence, larger delay times [1, 21].

Additionally, the model of Jirsa and Haken assumes no delay between the conversion

of incoming pulses at target synapses to dendritic potentials and back-conversion to outgoing pulses. Since it is known from physiological studies that synapses respond to incoming pulses by convolution with an impulse function causing delay effects, we extend the model equations by an additional dendritic delay.

A dendritic delay was already considered in previous work by Wright et al. [22, 23, 24, 25] for intercortical connections. There, the inhibitory connections are assumed being local and only the excitatory connections render the system nonlocal in space. This nonlocality is then approximated by a local model based on a wave equation. In contrast, we shall examine the situation where both interactions can have a finite range and include the full nonlocalities in space as well as in time in our model.

In addition, we would like to point to a fundamental difference between both model approaches. Wright and colleagues distinguish excitatory and inhibitory pulse activity, which sum up at synapses, while our model assumes summation of excitatory and inhibitory postsynaptic potentials at the soma. Both assumptions yield different field equations and corresponding mathematical treatments, but are on a par.

The paper is structured as follows: the next section presents the extended equations and a reduction of the model to a single integro-differential equation with delay. In the subsequent sections, a stability analysis of a one-dimensional spatially homogeneous stationary state exhibits conditions for Turing [26] and oscillatory or Hopf instabilities [27]. To obtain a Hopf instability it turns out that the propagation velocity has to be constrained to a certain finite interval, which depends on biological parameters. A brief study of the phase velocity of occuring travelling waves is supplemented. The last section presents numerical solutions for special parameter values.

2 Derivation of field equation

Pyramidal neurons generate action potentials, if their somatic membrane potential exceeds an intrinsic threshold. The generated pulses propagate on axonal fibres and terminate at synapses of adjacent neurons. Chemical synapses respond to incoming pulse activity by potential changes, which propagate on dendrites to the soma of the neuron, where they sum up to an effective membrane potential. The time scale of axonal pulses is $\sim 1ms$, while postsynaptic potentials on the dendrites are slower by a rough factor of 10.

The description of dynamics in neural nets is rather superficial, as there are more detailed and complex mechanisms in single neurons [28, 29, 30]. However, we do not consider these aspects, as these mechanisms are observed mainly at the single-neuron level. Since neurons are highly interconnected [31, 32] and show a lack of connection specificity, the notion of a neural mass has been introduced [33, 34]. For sufficiently dense synaptic interactions, neural masses exhibit cooperative dynamical behavior and are rather independent from inner dynamics. Hence, corresponding neuronal field theories comprise properties of neuronal ensembles at a specific hierarchical

2

level. In the following, we consider time course-grained activity of neural volume elements and connections between them. Since thresholds of single neurons in a neuronal ensemble obey a distribution, a mean threshold and corresponding variance determine the new conversion relations of membrane potentials and pulse rates [35]. Measurements indicate that the conversion from mean membrane potentials V to puls rates P obey a sigmoid function S [36]. In a continuous neuronal field, we obtain

$$P(x,t) = S_{\max}S[V(x,t)] = \frac{S_{\max}}{1 + e^{-c(V(x,t)-V_r)}} \; ,\tag{1}$$

with the maximum pulse rate $S_{\max}$ and the values $c = 1.82$ and $V_r = 3$ taken from the literature [22]. This formulation assumes identical neurons, which only differ by their synaptic properties. Several works used this assumptions implicitly [1, 15, 17, 33, 34], while others distinguish between excitatory and inhibitory neurons [3, 23]. Corresponding to the single neuron-level, pulse activity propagates along axonal fibres and terminate at synapses, which either excite (e) or inhibit (i) the target neuron. The entering pulse rate in excitatory and inhibitory synapses reads in one spatial dimension

$$\bar{P}_{e,i}(x,t) = \int_\Gamma dx' \beta_{e,i} f_{e,i}(x,x') P(x', t - \frac{|x-x'|}{v_{e,i}}) + \mu_{e,i} P^{ext}(x,t) \; .\tag{2}$$

Here, we introduce synaptic connection probability distributions $f_{e,i}$ and corresponding weight factors $\beta_{e,i}$. The considered delay term originates from a finite pulse propagation velocity $v_{e,i}$. Additionally, an external pulse activity P^{ext} is considered with corresponding coupling constants $\mu_{e,i}$. The response of chemical synapses to incoming pulse activity can be described by a convolution with the impulse response function $h_{e,i}(t)$ for excitatory and inhibitory postsynaptic potentials

$$V_{e,i}(x,t) = g_{e,i} \int_{-\infty}^t d\tau h_{e,i}(t-\tau) \bar{P}_{e,i}(x,\tau) \; ,\tag{3}$$

where $g_{e,i}$ denote excitatory and inhibitory synaptic gain factors, respectively. These potentials are transients of membrane potentials and sum up to an effective membrane potential $V = V_e - V_i$. At last, we assume

- identical impulse response functions of excitatory and inhibitory synapses, i.e. $h_e = h_i = h$, and identical wave-pulse conversion functions $S_e = S_i = S$ for all cells,

- only intracortical connections by un-myelinated axonal fibres and common propagation velocity $v_e = v_i = v$,

- only excitatory input $P^{ext} = P$, $\mu_i = 0$ and

3

- isotropic and homogeneous synaptic connections.

Combination of equations (1), (2) and (3) yields

$$V_e(x, t) = \int_{-\infty}^{t} d\tau h(t - \tau) \left\{ \int_{\Gamma} dx' a_e f_e(x, x') S[V(x', \tau - \frac{|x - x'|}{v})] + \mu P(x, \tau) \right\}$$

$$V_i(x, t) = \int_{-\infty}^{t} d\tau h(t - \tau) \int_{\Gamma} dx' a_i f_i(x, x') S[V(x', \tau - \frac{|x - x'|}{v})]$$

with $a_{e,i} = g_{e,i} \beta_{e,i} S_{\max}$, $\mu = g_e \mu_e$. We obtain

$$V(x, t) = \int_{-\infty}^{t} d\tau \int_{\Gamma} dx' \ h(t - \tau) \tag{4}$$

$$\times \quad \left\{ (a_e f_e(x, x') - a_i f_i(x, x')) S[V(x', \tau - \frac{|x - x'|}{v})] + \mu P(x, \tau) \right\}$$

Studies of synaptic mechanisms indicate the impulse response function [21]

$$h(t) = \frac{\alpha_1 \alpha_2}{\alpha_1 - \alpha_2} (\exp[-\alpha_1 t] - \exp[-\alpha_2 t]), \qquad \alpha_1, \alpha_2 > 0 \ ,$$

which can be interpreted as a Greens function for the second order linear differential operator

$$\hat{L} = (\frac{\partial}{\partial t} + \alpha_1)(\frac{\partial}{\partial t} + \alpha_2) \ ,$$

obeying

$$\hat{L} h(t) = \delta(t) \tag{5}$$

with $\delta(t)$ being the delta-function. In addition, we like to mention the case $\alpha_1 = \alpha_2 = \alpha$, which simplifies the impulse response function to $\alpha^2 t \exp(-\alpha t)$, then called *alpha-function*.

For the specific synaptic connectivity functions we assume exponential decay in space

$$f_{e,i}(x, x') = \frac{1}{2r_{e,i}} \exp[-|x - x'|/r_{e,i}].$$

4

Applying $\hat{L}$ to (4) and using (5), we obtain after scaling $t \to t\sqrt{\alpha_1 \alpha_2}$, $x \to x/r_e$, $v \to v/(r_e\sqrt{\alpha_1 \alpha_2})$ the final field equation

$$\hat{L}V(x, t) = \left[\frac{\partial^2}{\partial t^2} + (\alpha + \frac{1}{\alpha})\frac{\partial}{\partial t} + 1\right]V(x, t)$$

$$= \frac{1}{2}\int_\Gamma dx' \left(a_e \exp[-|x - x'|] - a_i r \exp[-|x - x'|r]\right)$$

$$\times S[V(x', t - \frac{|x - x'|}{v})] + \mu P(x, t) \qquad (6)$$

with $\alpha = \sqrt{\alpha_1/\alpha_2}$ and $r = r_e/r_i$. The excitatory and inhibitory connection parameters r_e and r_i determine spatial scales, while α and v introduce different temporal scales.

In case of $a_e > a_i$, the synaptic connectivity function looks like a mexican hat for $r < 1$ and reversed for $r > 1$ (cf. figure 3). The latter case or, more generally speaking, couplings of local-inhibition lateral-excitation type are common in many cortical areas if the axonal and dendritic arborizations of neurons tangential to the cortical surface are considered [37, 38, 39, 40]. Roughly speaking the dendritic arborizations of excitatory and inhibitory cells are comparable extending more or less homogeneously over an area with radius in the range of up to a few hundred micrometers. Axonal fibres of inhibitory neurons roughly cover the same area. In contrast, excitatory cells, and in particular large pyramidal neurons, reveal axonal arborizations that can extend over up to a few millimeters, where the probability of connections decays with distance from the cell. It is further commonly assumed that local inhibition is stronger than local excitation (for instance, because pharmacological disinhibition of the cortex easily leads to epileptic activity). Thus, the lateral cortical connectivity in space seems to be basically of local-inhibition lateral-excitation type. Although the excitatory long-range connections are known to be in part 'patchy' — that is synaptic contacts are not formed homogeneously in space, but cluster in many small areas of a few hundred micometers in diameter [41, 42] — the inverse Mexican hat nonetheless seems to be a good aproximation to study activation patterns arising from such a connectivity scheme.

Lateral inhibition is a phenomenon similarly prominent in neural systems, although in a somewhat different context. Neurons in sensory systems of many species are 'tuned' to certain stimulus features present on the sensory surface, e.g., to the location of dots or the orientation of bars in the visual domain, to tones in auditory areas, or to the location of touch in the somato-sensory system. It is known since long (e.g., [43]) that simultaneously applied stimuli which slightly differ with respect to the feature dimension under consideration, suppress activity in a recorded cell as compared with the response to an optimal stimulus alone [39, 40]. This effect is believed to arise from lateral inhibition and serves to sharpen tuning functions of cortical neurons relative to the tuning of their afferent fibres. More recently it has been proposed that in primary cortical areas, sharply tuned and strong excitatory

couplings play an additional role in the generation of sharp tuning curves [44, 45, 46]. These theories emphasize Mexican hat type (local-excitation lateral-inhibition) coupling schemes, however, observe that the couplings here are functional connectivities in some feature domain, which does not necessarily map to physical space on the cortical surface. Nonetheless, nearby neurons in many cortical areas often code for similar stimulus features. Therefore, it seem reasonable to assume distance dependent delays also in these functional models.

In the subsequent sections, we study the influence of parameters r, α and v on the field stability and spatio-temporal pattern formation out of equilibrium described by (6).

3   Stability of a homogeneous rest state

It is well known that self-organized, spatio-temporal pattern formation may occur in systems out of equilibrium if a spatially and temporally homogeneous state looses stability [47, 48]. This was also demonstrated in biological systems [19]. To examine our model with respect to the emergence of such patterns, we apply a linear stability analysis in this section. For a stationary, homogeneous external excitation

$$P(x, t) = P_0$$

and an infinitely extended or periodic spatial field, equation (6) has the constant solution (rest state) V_0 determined by the transcendent equation

$$(a_e - a_i) S(V_0) - V_0 + \mu P_0 = 0 , \tag{7}$$

which can be solved numerically. The existence of a fixed point in the active part of the sigmoid function yields the restriction $a_e > a_i$ (figure 1). There are indications, that inhibitory gain factors can exceed excitatory gain factors [31], which might lead to $a_e < a_i$. However, we neglect this case in the present work and shall assume $a_e > a_i$ for the rest of the paper. Additionally, the condition

$$\left. \frac{dS}{dV} \right|_{V=V_0} < \frac{1}{a_e - a_i}$$

ensures stability of the rest state. In order to determine the influence of the various parameters entering in equation (6), especially the one of the propagation velocity v on the stability of the rest state V_0, we shall perform a linear stability analysis with respect to spatially varying disturbances:

$$V(x, t) = V_0 + \int dk \, u_k \mathrm{e}^{ikx + \lambda(k)t}. \tag{8}$$

By inserting equation (8) into equation (6), it turns out that the equations for different wave vectors k decouple, leading to a characteristic polynomial of sixth order for the growth rate λ (for sake of simplicity we put $\alpha = 1$, corresponding to $\alpha_1 = \alpha_2$):

$$\lambda^2 + 2\lambda + 1 - \gamma \left[\frac{1 + \lambda/v}{k^2 + (1 + \lambda/v)^2} a_e - \frac{r + \lambda/v}{k^2 + (r + \lambda/v)^2} r a_i \right] = 0, \qquad (9)$$

where γ denotes the derivative of S at the "operating point" which can be modified by changing P_0 (figure 1):

$$\gamma = \frac{dS}{dV}\bigg|_{V=V_0}$$

Due to the unique dependence of γ on P_0 we may also choose γ as control parameter instead of the external stimulus P_0.

According to the common classification of spatio-temporal instabilities in extended systems (see e.g. [47, 48]), we may determine several important cases. The most simplest one is that of a monotonic instability, which usually leads to stationary but spatially inhomogeneous patterns. We shall discuss these patterns here briefly.

The monotonic instability of the homogeneous state is obtained by the condition

$$\lambda = 0 .$$

From equation (9) the critical γ_c where λ changes its sign then reads

$$\gamma_c(k) = \frac{r^2 + (1 + r^2)k^2 + k^4}{(a_e - a_i)r^2 + (a_e - a_i r^2)k^2} \qquad (10)$$

A homogeneous ($k = 0$) monotonic instability is obtained if

$$\gamma_c > \frac{1}{a_e - a_i}$$

which obviously contradicts the condition for the stability of the rest state. But for the case of local excitation and lateral inhibition, i.e. $r < 1$ (cf. figure 3(a)), equation (10) can have a minimum less than $1/(a_e - a_i)$ at a certain finite k (figure 2). A more detailed investigation shows that such a minimum occurs for

$$r^2 < \frac{a_i}{a_e}$$

at critical wave vectors that behave for small r like $\sqrt{r}$. This is nothing but the Turing instability known from non-equilibrium activator-inhibitor systems [26]. Its

7

occurrence in chemistry is linked to the condition that the inhibitor must propagate much faster than the activator [49]. In the frame of our model, small r means $r_e < r_i$, the range of excitatory interaction has to be smaller than that of inhibition.

A more complicated case is that of an oscillatory (Hopf) instability of the rest state, where the non-linear solution is expected to be an intrinsic time and space dependent function. Different to the Turing case, a local inhibition and lateral excitation is necessary, i.e. $r > 1$ (cf. figure 3(b)). If it occurs first with $k \neq 0$, this instability is sometimes called "wave instability". Even in the weakly nonlinear regime, complex structures of traveling or standing wave types are expected. In the monotonic case, the delay time and therefore the propagation velocity v plays, at least for the eventually reached steady states, no role. In the oscillatory case, v acts as another important control parameter, what we shall show now.

Inserting

$$\lambda = i\omega$$

into equation (9) gives the two conditions

$$
\begin{aligned}
\omega^6 + b_4\omega^4 + b_2\omega^2 + b_0 &= 0 & (11) \\
b_5\omega^4 + b_3\omega^2 + b_1 &= 0, & (12)
\end{aligned}
$$

which holds on the critical line $\text{Re}(\lambda) = 0$. The coefficients b_i are algebraic expressions of the wave vector and the parameters of equation (9):

$$b_i = b_i(k^2, r, \gamma, v, a_e, a_i)$$

Now we fix the values of γ by an external stimulus and consider the ratio r of excitatory and inhibitory ranges as control parameter. The second free parameter is the propagation velocity v. For the sake of simplicity, we additionally fix a_e, and a_i to certain values and find from equation (12)

$$\omega = \omega(k^2, r, v)$$

which yields, inserted into (11), the stability lines

$$r = r(v, k_c^2)$$

in the $v-r$-plane. Here k_c denotes the wave vector which belongs to the mode getting unstable first. It turns out, that k_c is always finite and the oscillatory instability has also a typical length scale (wave instability). Figure 4 shows a part of the parameter

8

plane together with the Turing region, which is independent from v. One recognizes a threshold for v, beyond which no oscillations exist.

Figure 5 outlines the dependence of the real and imaginary parts of $\lambda = \Lambda + i\omega$ on the wave vector near the instability limit. The parameters are $r = 10$ and $v = 1.2$. From these computations one may deduce the phase velocity of the traveling waves at onset of instability, according to

$$v_{ph} = \frac{\omega(k_c)}{k_c} \ .$$

The result is shown for several values of the propagation velocity v in figure 6. One recognizes, that for larger values of v the phase velocity differs more and more from the propagation velocity and the phase velocity of traveling waves decreases significantly. This can be understood on a qualitative level by the fact that the dendritic delay represented by the form of $h(t)$ in equation (3) slows down the effective propagation velocity. This effect becomes more prominent for a higher propagation velocity v, as for small v the delay of the activity due to transmission from one part of the neuronal ensemble to another is much larger than the delay coming from the dendritic dynamics. The obtained values of v_{ph} correspond well to measured intracortical wave propagation velocities in visual cortex [50].

We conclude this section by a brief discussion of the new features of our model compared to others. Due to the inclusion of the synaptic delay, our model has two characteristic time scales, namely the synaptic delay and the delay caused by activity propagation. In contrast to the nonlocal equations studied by Jirsa et al. [15], where the first effect was neglected and no time derivatives are included, the size of v may change the behavior of the system qualitatively. It cannot be scaled away using a different time scale and therefore plays the role of an additional control parameter.

On the other hand, it is obvious from our calculations, that if the propagation delay due to propagation is neglected ($v \to \infty$), an oscillatory instability would not longer be possible (cf. figure 4). Only the Turing patterns discussed above could be obtained in that case.

4 Numerical results

4.1 The method

In this part we wish to present some direct numerical solutions of equation (6). To this end we rewrite it into the form of two coupled first order differential equations ($\alpha = 1$):

$$\partial_t V(x,t) = \Phi(x,t) \tag{13}$$

$$\partial_t \Phi(x,t) = -2\Phi(x,t) - V(x,t) + J(x,t) + \mu P(x,t) \tag{14}$$

where $J(x, t)$ stands for the integral on the left hand side of equation (6) and includes all non-linearities as well as all non-local effects. Further, we continue the integration region L periodically. From equation (6) we see that J is composed of two integrals, each having the form

$$
\begin{aligned}
I(x, t) &= \int_{x-L/2}^{x+L/2} dx' \, F(x', t - \frac{|x - x'|}{v}) \exp[-\eta|x - x'|] \\
&= \int_0^L du \, (F(x - u, t - u/v) + F(x + u, t - u/v)) \exp[-\eta u] \quad (15)
\end{aligned}
$$

To evaluate this expressions further numerically, we introduce a grid in real space with $N + 1$ mesh points having equal distances Δu and $L = N\Delta u$. Then (15) can be written as the sum

$$
I(x, t) = \int_0^L du \, G(x, u, t) \exp[-\eta u] = \sum_{n=0}^{N-1} \int_{u_n}^{u_{n+1}} du \, G(x, u, t) \exp[-\eta u] \quad (16)
$$

over the small intervals Δu. Here, we used the abbreviation

$$
G(x, u, t) = [F(x - u, t - u/v) + F(x + u, t - u/v)]
$$

and $u_n = n\Delta u$. For small enough Δu, G may not vary much in each interval and can be approximated by a linear function of u:

$$
G(x, u, t) \approx G(x, u_n, t) + \frac{G(x, u_{n+1}, t) - G(x, u_n, t)}{\Delta u}(u - u_n) \qquad u_n \le u \le u_{n+1}
$$

Inserting this into (16) leads finally after integration to the formula

$$
\begin{aligned}
I(x, t) &\approx \frac{1}{\eta^2 \Delta u} \sum_{n=0}^{N-1} \exp[-\eta u_{n+1}][G(x, u_{n+2}, t) - 2G(x, u_{n+1}, t) + G(x, u_n, t)] \\
&\quad + \frac{1}{\eta} \left[G(x, 0, t) + \frac{G(x, \Delta u, t) - G(x, 0, t)}{\eta \Delta u} \right] - K
\end{aligned}
$$

where K is a correction of $O(\exp[-\eta L])$

$$
K = \frac{1}{\eta} \exp[-\eta L] \left[G(x, L, t) + \frac{G(x, \Delta u, t) - G(x, L, t)}{\eta \Delta u} \right]
$$

coming from the finite length L. Note that this scheme yields the exact result $I = G/\eta - K$ for the case of a constant G.

The time derivatives in (13), (14) can be approximated by first order differential formulas, leading to an Euler-forward scheme in time.

4.2 Turing patterns

We begin the numerical studies computing a time series in the Turing regime. From the linearized equations we expect a transient behavior to an eventually stationary,

spatially periodic excitation pattern. For the parameters we used $a_e = 6$, $a_i = 5$, $r_e = 0.5$mm and $r_i = 1.0$mm. The x-axis, having the total length $L = 5$cm, was divided into 400 mesh intervals. The time step for the Euler-forward integration was fixed at $\Delta t = 0.05$. For the propagation velocity we tried several values in the range between 0.0025[m/s] and 0.25[m/s]. For rescaling the velocity to physical units, one needs values for the frequencies α_i. We took $\alpha_1 = \alpha_2 \approx 400 s^{-1}$ from [23]. We found that there is no influence of the velocity on pattern formation in the Turing regime.

Figure 7 shows the occurrence and stabilization of a periodic Turing structure. As initial condition we chose a randomly distributed field. For the external stimulus we used a constant value of $\mu P = \mu P_0 = 2.5$ (cf. figure 1). Note that the time is given in dimensionless units. To obtain the real time, this has to be multiplied by $1/\sqrt{\alpha_1 \alpha_2} = (1/400)$s and the stabilization of the structure would take about 0.2 seconds. The typical length scale of the structure is in the range of some mm, somewhat larger but comparable to the size of the connections $r_{e,i}$.

4.3 Waves

Next we turn to the oscillatory regime which is obtained for $r_e > r_i$. The generic pattern consists of more or less regular traveling waves. We distinguish between homogeneous and inhomogeneous external stimuli, as well as between parameters close to and well above threshold. For all runs presented below we fixed $r_e = 1$mm and $v = 0.16$m/s. The length of the layer is now $L = 1.5$cm.

4.3.1 Homogeneous external stimulation

Figure 8 shows the onset of traveling waves slightly above instability of the homogeneous state. Again we used the value $\mu P = \mu P_0 = 2.5$ for the external stimulation. After a short transient phase of standing waves, traveling waves are obtained, which propagate with the phase velocity close to the one found from the linear problem. The amplitude saturates after $t = 200$, corresponding to $t = 0.5$s. For this run we chose $r = 2.8$, close above the corresponding instability line in figure 4.

We note that non-periodic boundary conditions could change the behavior at least near the boundaries and that an interplay between waves and reflected waves could lead to more involved patterns. Studies of the system with different boundaries as well as a two-dimensional extension is currently in progress.

Figure 9 shows a situation well above onset for $r = 10$ and larger $a_{e,i}$. From pattern formation in non-equilibrium systems like fluids or chemical reactions [48] it is well-known that non-periodic solutions (defects, grain boundaries in higher dimensions) may occurre well above threshold, whereas regular (periodic) structures are usually close to the onset of instability. The same behavior can be observed here. The initial transient phase is now completely different and consists of standing waves with an irregular but quite large wave length. Then traveling waves invade the whole region,

11

but localized defects remain. These defects move in the opposite direction of the waves and with a much slower velocity. In that way the system is able to store information and may act as a dynamic memory. In the next paragraph, we show how this information can be erased by an external localized stimulus.

4.3.2 Inhomogeneous external stimulation

Next we allow for a strong but spatially localized external stimulus of the form

$$\mu P(x,t) = \begin{cases} \mu P_0 + Q(t), & 0.475L \le x \le 0.525L \\ \mu P_0, & \text{else} \end{cases}$$

where $\mu P_0 = 2.5$ and $Q(t)$ can be switched on and off in time to a value of 20.

Figure 10 shows pattern formation close to threshold with a constant stimulus switched on from the beginning, while all parameters are the same as in figure 8. Due to the inhomogeneity, the patterns are now standing waves instead of traveling waves. This is an evident example how a local stimulation may change the global behavior of the structure. Switching off the stimulation would lead to a transient to traveling waves.

In figure 9 we found the formation and storage of topological defects in a traveling wave pattern well above threshold. Now we wish to study the influence of a localized stimulus in space and time onto such a pattern. In figure 11 we used a three-defect state and switched on a localized stimulus at $t = 45$. The stimulus erases the defects and after switching it off at $t = 130$, a regular traveling wave pattern remains. We also found solutions where a stimulus produces topological defects which remain in the system after switching it off. A more detailed analysis of the stimulus shape and time course on the creation and annihilation of defects is left for the future.

5   Conclusions

The present work proposes a field model for intracortical activity based on a previously developed model for long-range interactions. The derived single field equation comprises both excitatory and inhibitory contributions. It considers two spatial scales expressed by the ratio of excitatory and inhibitory connection ranges and two time scales defined by synaptic response and axonal propagation delay. An analytical stability analysis for a stationary state homogeneous in space yields conditions for different pattern instabilities. It is shown analytically for spatially constant external stimuli that near onset of instability local excitation and lateral inhibition enables Turing patterns, while oscillatory instabilities can occur in the case of local inhibition and lateral excitation. Numerical simulations confirm these findings. In addition, it turns out, that oscillatory instabilities only occur beyond a certain delay threshold. In contrast, Turing patterns are observed being independent from delay effects. Inspection of the observed phase velocity of waves shows its increase with

decreasing slope with increasing propagation velocity. Simulations exhibit phase velocities similar to measured activity propagation velocities. Finally, numerical simulations subject to non-constant external stimuli and far from equilibrium exhibit more complex patterns as travelling defects and multi-frequency waves.

The proposed model exhibits self-organized pattern formation subject to an external stimulus. Hence, it might represent a generic model for single neuronal entities, which might be combined to model networks. However, future work is necessary, concerning the influence of boundary conditions. A two-dimensional formulation and 2D numerical solutions are desirable, as well as further studies on effects of non-constant external stimuli. An important future aspect will be the comparison to experimental data. This step is regarded crucial and might be attacked by studies of frequency power spectra or electromagnetic forward solutions.

6 Acknowledgements

References

[1] P.L. Nunez. *Neocortical dynamics and human EEG rhythms*. Oxfoord University Press, New York - Oxford, 1995.

[2] J.J. Wright and R.R. Kydd. The electroencephaloggram and cortical neural networks. *Network*, 3:341–362, 1992.

[3] J.J. Wright and D.T.J. Liley. Dynamics of the brain at global and microscopic scales: Neural networks and the eeg. *Behavioral and Brains Sciences*, 19:285–320, 1996.

[4] P.C. Bressloff and S. Coombes. Physics of the extended neuron. *International Journal of Modern Physics B*, 11(20):2343–2392, 1997.

[5] B. Ermentrout. Neural networks as spatio-temporal pattern-forming systems. *Reports on Progress in Physics*, 61:353–430, 1998.

[6] A.K. Sturm and P. König. Mechanisms to synchronize neuronal activity. *Biological Cybernetics*, 84:153–172, 2001.

[7] D. Golomb and G.B. Ermentrout. Effects of delay on the type and velocity of travelling pulses in neuronal networks with spatially decaying connectivity. *Network: Comput. Neural Syst.*, 11:221–246, 2000.

[8] D. Golomb and G.B. Ermentrout. Bistability in pulse propagation in networks of excitatory and inhibitory populations. *Physical Review Letters*, 86(18):4179–4182, 2001.

[9] D. Golomb and G.B. Ermentrout. Slow excitation supports propagation of slow pulses in networks of excitatory and inhibitory populations. *Physical Review E*, 65:061911, 2002.

[10] R. Osan and G.B. Ermentrout. The evolution of synaptically generated waves in one- and two-dimensional domains. *Physica D*, 163:217–235, 2002.

[11] W.M. Kistler, R. Seitz, and J.L. van Hemmen. Modeling collective excitations in cortical tissue. *Physica D*, 114:273–295, 1998.

[12] H. Haken. Effect of delay on phase locking in a pulse coupled neural network. *European Physical Journal B*, 18:545–550, 2000.

[13] H. Haken. Delay, noise and phase locking in puls coupled neural networks. *Biosystems*, 63:15–20, 2001.

[14] J.J. Wright and D.T.J. Liley. A millimetric-scale simulation of electrocortical wave dynamics based on anatomical estimates of cortical synaptic density. *Biosystems*, 63:15–20, 2001.

[15] V.K. Jirsa and H. Haken. Field theory of electromagnetic brain activity. *Physical Review Letters*, 7(5):960–963, 1996.

[16] V.K. Jirsa and H. Haken. A derivation of a macroscopic field theory of the brain from the quasi-microscopic neural dynamics. *Physica D*, 99:503–526, 1997.

[17] T.D. Frank, A. Daffertshofer, P.J. Beek, and H. Haken. Impacts of noise on a field theoretical model of the human brain. *Physica D*, 127:233–249, 1999.

[18] V.K. Jirsa, K.J. Jantzen, A. Fuchs, and J.A.S. Kelso. Spatiotemporal forward solution of the eeg and meg using network modelling. *IEEE Transactions on Medical Imaging*, 21(5):493–504, 2002.

[19] S. Amari. Dynamics of pattern formation in lateral-inhibition type neural fields. *Biol. Cybernetics*, 27:77–87, 1977.

[20] T. Wennekers. Dynamic approximation of spatio-temporal receptive fields in nonlinear neural field models. *Neural Computation*, 14:1801–1825, 2002.

[21] P. Dayan and L.F. Abbott. *Theoretical Neuroscience : Computational and Mathematical Modeling of Neural Systems*. MIT Press, 2001.

[22] J.J. Wright and D.T.J. Liley. Simulation of electrocortical waves. *Biological Cybernetics*, 72:347–356, 1995.

[23] P.A. Robinson, C.J. Rennie, and J.J. Wright. Propagation and stability of waves of electrical activity in the cerebral cortex. *Physical Review E*, 56(1):826–840, 1997.

[24] P.A. Robinson, P.N. Loxley, S.C. O'Connor, and C.J. Rennie. Modal analysis of corticothalamic dynamics, electroencephalographic spectra and evoked potentials. *Physical Review E*, 63:041909, 2001.

[25] C.J. Rennie, P.A. Robinson, and J.J. Wright. Unified neurophysical model of eeg spectra and evoked potentials. *Biological Cybernetics*, 86:457–471, 2002.

[26] A.M. Turing. The chemical basis of morphogenesis. *Philos. Trans. R. Soc. London*, 327B:37–72, 1952.

[27] Y. Kuramoto. *Chemical Oscillations, Waves, and Turbulence*. Springer, Berlin, 1984.

[28] B. Katz. *The Release of Neuronal Transmitter Substances*. Liverpool University Press, Liverpool, 1969.

[29] B.P. Bean. Classes of calcium channels in vertebrate cells. *Annual Review of Physiology*, 51:367–384, 1989.

[30] S. Coombes. The effect of ion pumps on the speed of travelling waves in the fire-diffuse-fire model of ca2+ release. *Bulletin of Mathematical Biology*, 63:1–20, 2001.

[31] V. Braitenberg and A. Schütz. *Cortex : statistics and geometry of neuronal connectivity.* Springer, Berlin - New York, 2nd edition edition, 1998.

[32] T.H. Bullock. Reassement of neural connectivity and its specification. In H.M. Pinsker and W.D. Willis, editors, *Information Processing in the Nervous System*, pages 119–220. Raven Press, New York, 1980.

[33] H.R. Wilson and J.D. Cowan. A mathematical theory of the functional dynamics of cortical and thalamic nervous tissue. *Kybernetik*, 13:55–80, 1973.

[34] W.J. Freeman. Tutorial on neurobiology: from single neurons to brain chaos. *International Journal of Bifurcation and Chaos*, 2(3):451–482, 1992.

[35] W.J. Freeman. Nonlinear gain mediating cortical stimulus-response relations. *Biological Cybernetics*, 33:237–247, 1979.

[36] W. Rall. A statistical theory of monosynaptic input-output relations. *J. Cell. Comp. Physiol.*, 46:373 –411, 1955.

[37] V. V. Braitenberg and A. Schüz. *Anatomy of the cortex.* Springer, Berlin, 1991.

[38] J. Fuster. *Memory in the cerebral cortex.* MIT Press, Boston, MA, 1995.

[39] E.R. Kandel, J.H. Schwartz, and T.M. Jessel. *Principles of neural science.* McGraw-Hill/Appleton and Lange, 4 edition, 2000.

[40] J.G. Nicholls, B.G. Wallace, P.A. Fuchs, and R.A. Martin. *From Neuron to Brain.* Sinauer Associates, Inc., Sunderland, MA, 4 edition, 2001.

[41] R. Malach. Cortical columns as devices for maximizing neuronal diversity. *Trends in Neuroscience*, 3:101–104, 1994.

[42] J.S. Lund, A. Angelucci, and P.C. Bressloff. Anatomical substrates for functional columns in macaque monkey primary visual cortex. *Cerebral Cortex*, 13:15–24, 2003.

[43] F. Ratliff. *Studies on excitation and inhibition in the retina.* Chapman and Hall, London, 1974.

[44] D.C. Somers, S.B. Nelson, and M. Sur. An emergent model of orientation selectivity in cat visual. *Journal of Neuroscience*, 15:5448–5465, 1995.

[45] R. Ben-Yishai, R.L. Bar-Or, and H. Sompolinsky. Theory of orientation tuning in visual cortex. *Proc.Natl.Acad.Sci.*, 92:3844–3848, 1995.

[46] D. Ferster and K.D. Miller. Neural mechanisms of orientation selectivity in the visual cortex. *Annual Review of Neuroscience*, 23:441–471, 2000.

[47] H. Haken. *Advanced Synergetics*. Springer, Berlin, 1983.

[48] M.C. Cross and P.C. Hohenberg. Pattern formation outside of equilibrium. *Reviews of Modern Physics*, 65(3):851–1114, 1993.

[49] V. Castets, E. Dulos, J. Boissonade, and P. De Kepper. Experimental-evidence of a sustained standing turing-type non-equilibrium chemical-pattern. *Phys. Rev. Lett.*, 64:2953–2956, 1990.

[50] V. Bringuier, F. Chavane, L. Glaeser, and Y. Fregnac. Horizontal propagation of visual activity in the synaptic integration field of area 17 neurons. *Science*, 283:695–699, 1999.

Figure 1: Graphic solution of equation (7). The intersection of the dashed lines with the sigmoid function yields the homogeneous solutions of the rest state.

Figure 2: Critical γ_c necessary for a Turing instability of the rest state for several values of $r = r_e/r_i$. At that threshold, the selected pattern has the wave vector that corresponds to the minima of γ_c. For $r \geq 1$ no such minimum exists.

Figure 3: Two cases of synaptic connections with $K(|x - x'|) = a_e \exp[-|x - x'|] - a_i r \exp[|x - x'|r]$ (a) $r < 1$: the neuronal field excites locally and inhibits laterally. A Turing pattern is possible for the additional condition $r^2 < a_i/a_e$ (plot computed for $r = 0.25, a_e = 6, a_i = 5$). (b) r$\geq$1: the neuronal field shows local inhibition and lateral excitation. An oscillation instability is possible for additional conditions (see figure 4) (computed for $r = 10, a_e = 41, a_i = 40$).

Figure 4: Phase diagram of instabilities. An oscillatory instability is obtained for the propagation velocity in a certain interval. The Turing instability does not depend on v.

Figure 5: Growth rate (left) and frequency of the first critical mode with respect to its wave vector. Close to onset, a small band of modes will grow exponentially until nonlinear selection and saturation processes come into play.

Figure 6: Phase velocity v_{ph} of traveling waves versus propagation velocity v.

Figure 7: Occurrence of a Turing structure out of a random dot initial state. The time proceeds vertically. The parameters are $r_i = 0.001$m, $r_e = 0.0005$m, $a_i = 5$, $a_e = 6$, $v = 0.08$m/s.

Figure 8: An oscillatory state of traveling waves is found close to threshold for $r_i = 0.00037$m, $r_e = 0.001$m, $a_i = 40$, $a_e = 41$, $v = 0.16$m/s.

Figure 9: Well above threshold topological defects remain from the random initial pattern and are stored. They move slowly in opposite direction to the traveling waves. $r_i = 0.0001$m, $r_e = 0.001$m, $a_i = 100$, $a_e = 101$, $v = 0.16$m/s.

Figure 10: A localized external stimulus in the center of the region. For the same parameters as in figure 8 standing waves are obtained.

Figure 11: Topological defects in a state obtained with the parameters of figure 9 can be removed by switching on an external stimulation.
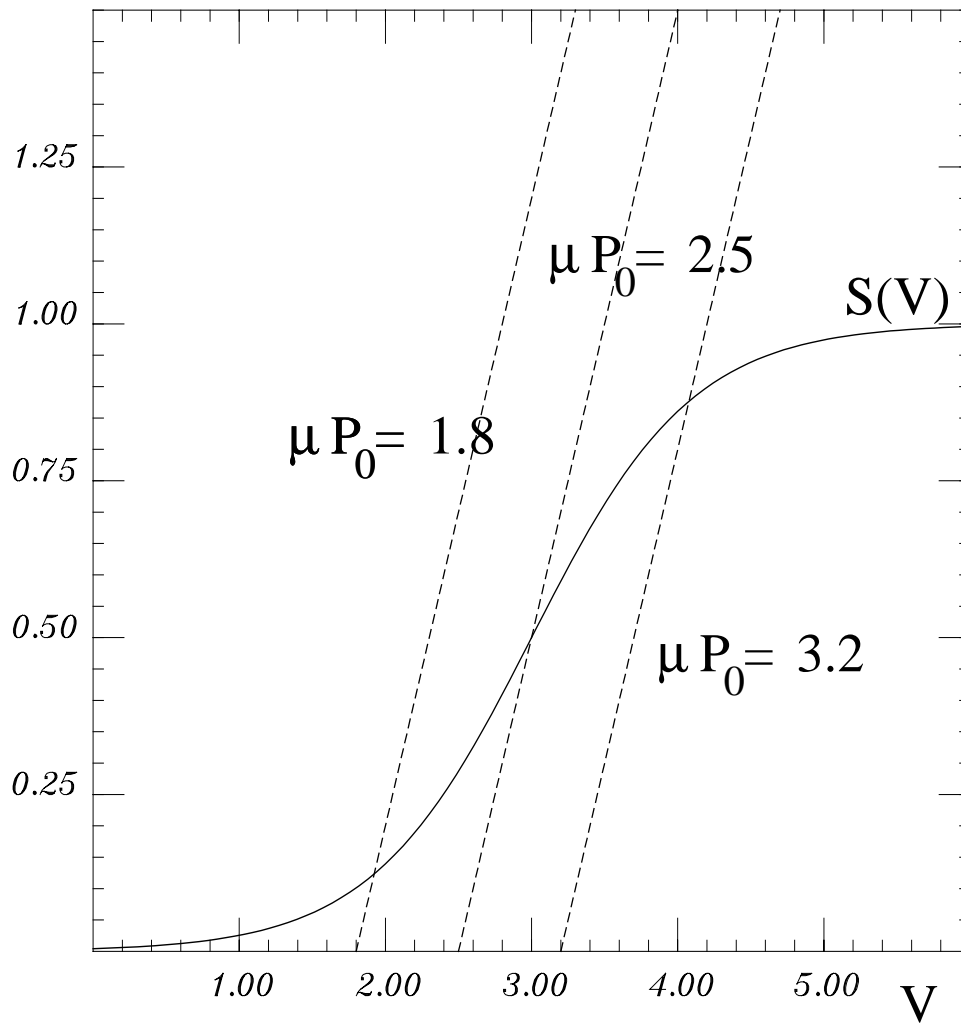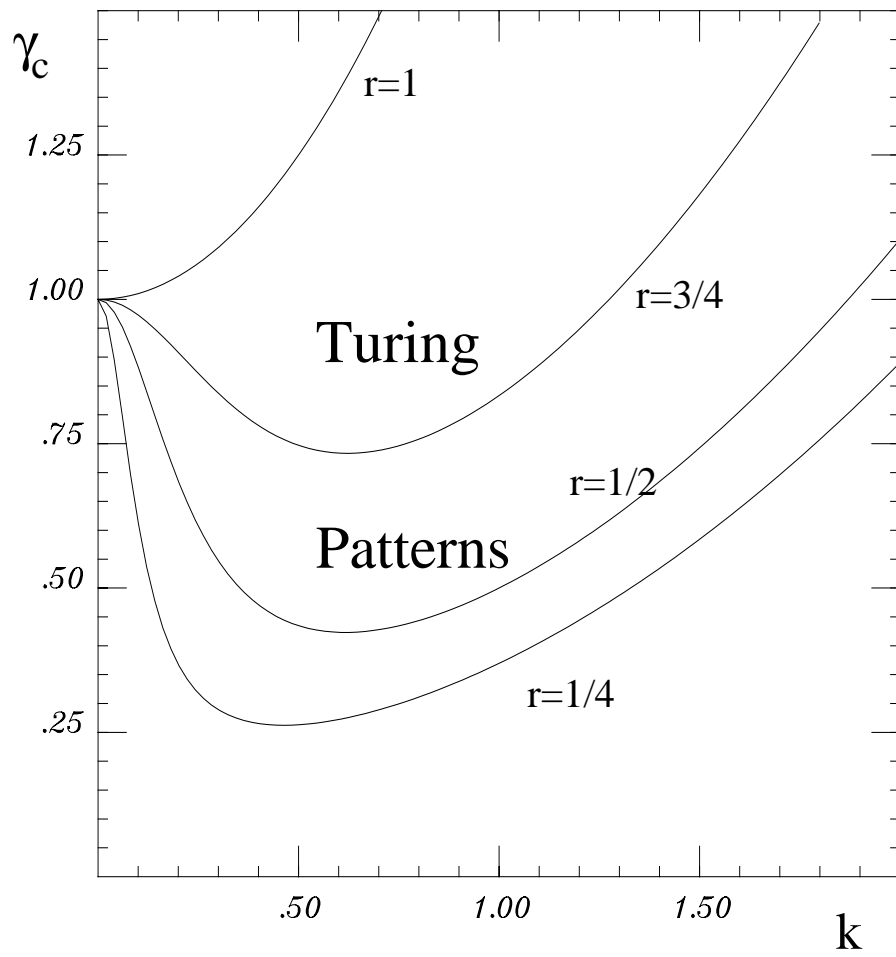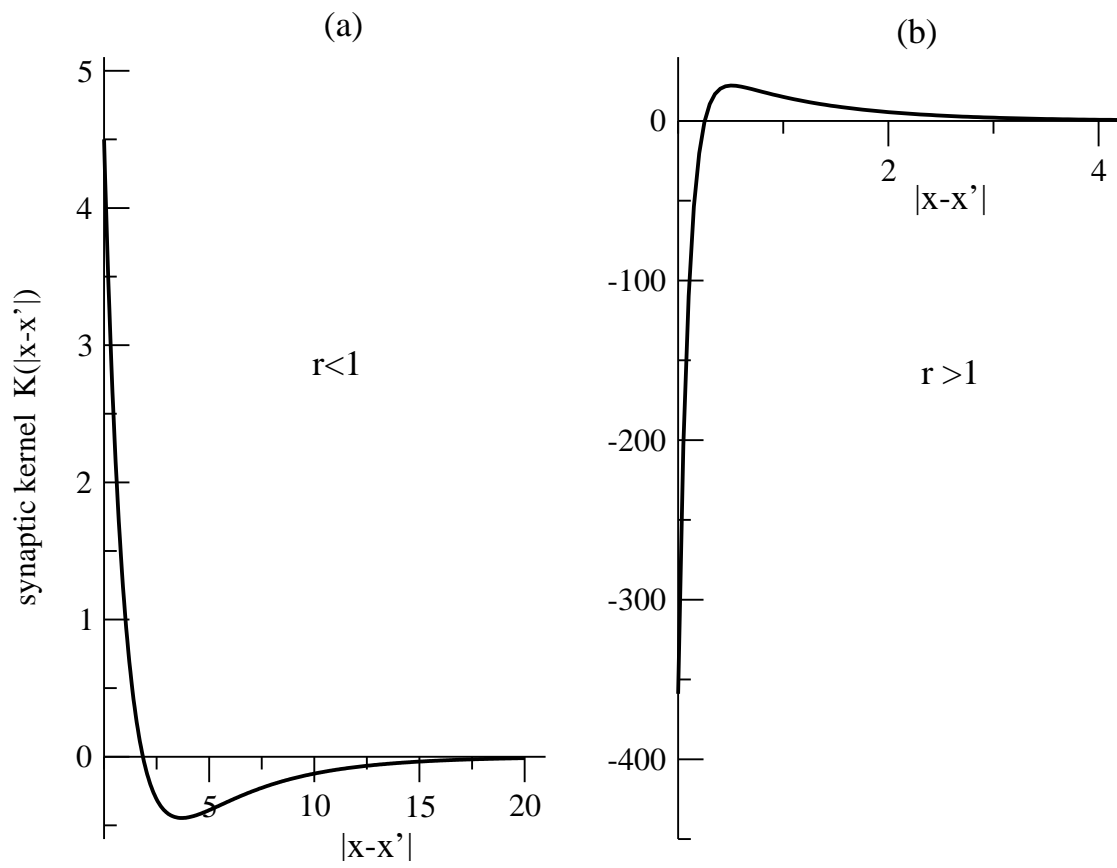
Figure 1

Figure 2
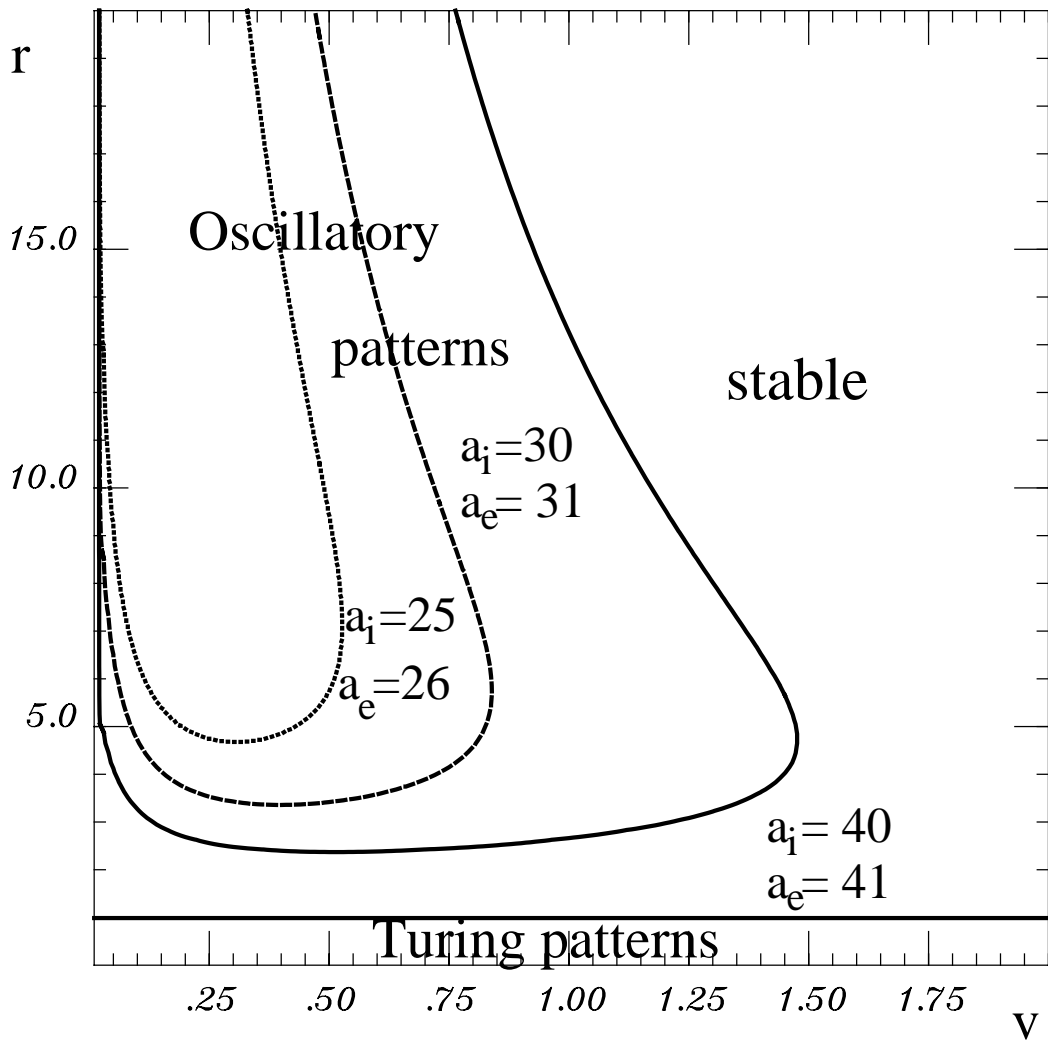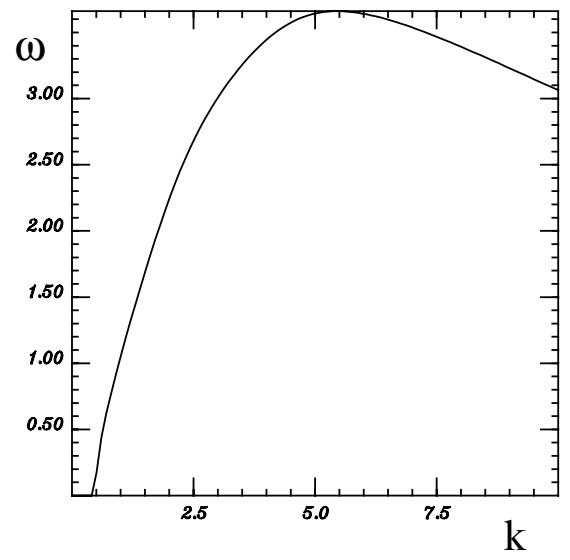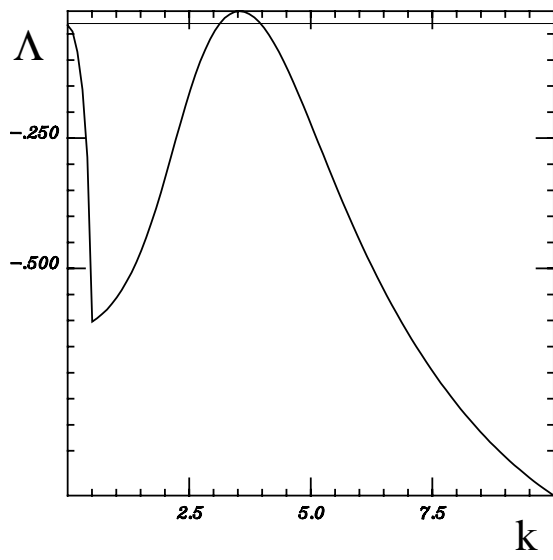
(a)

(b)

synaptic kernel K(|x-x'|)
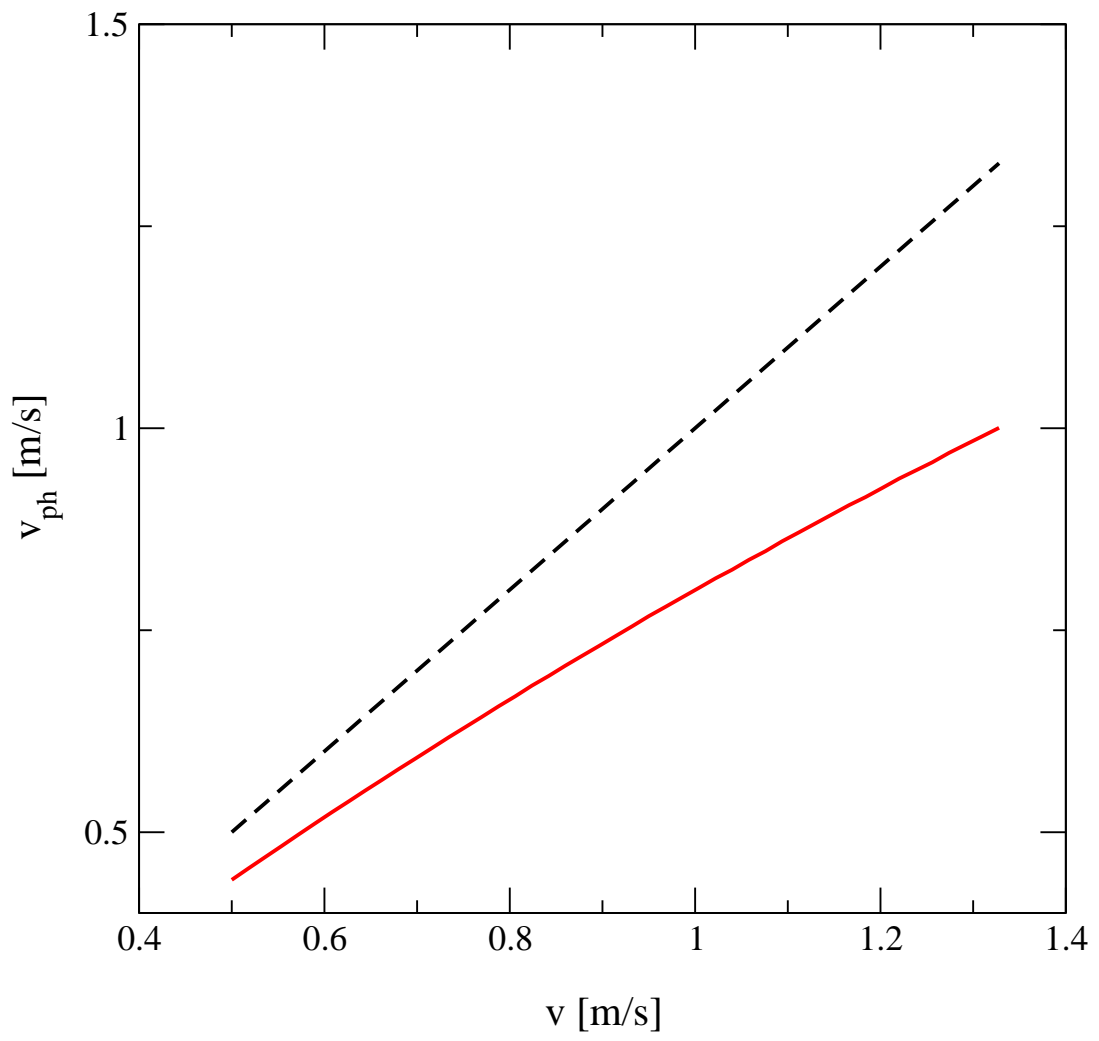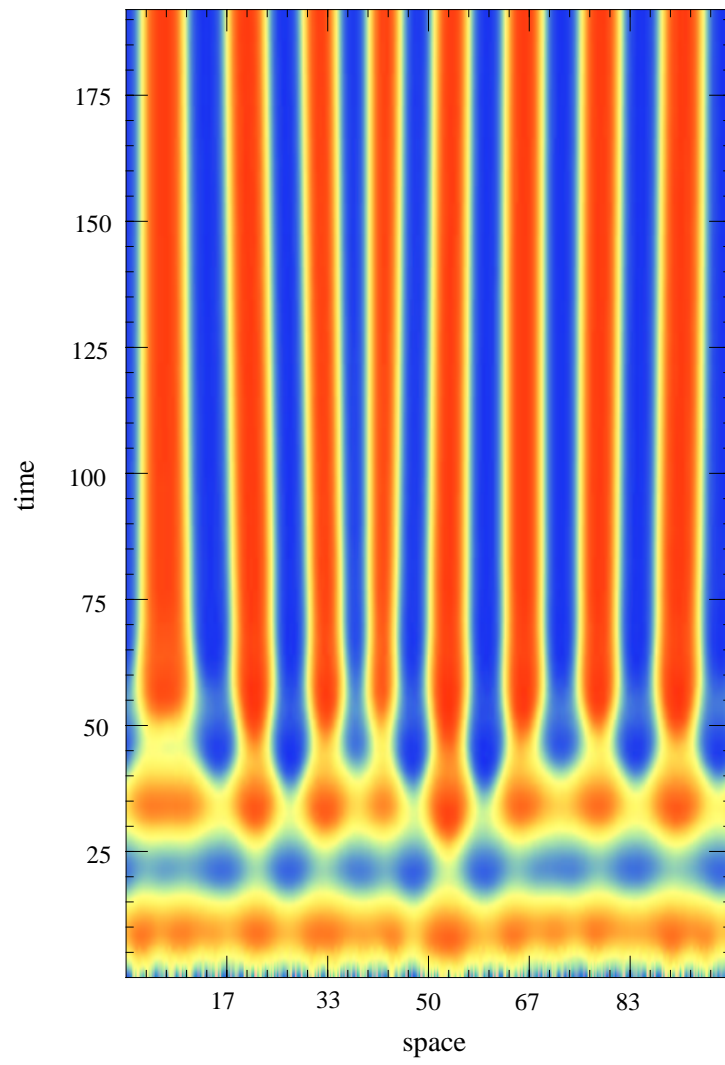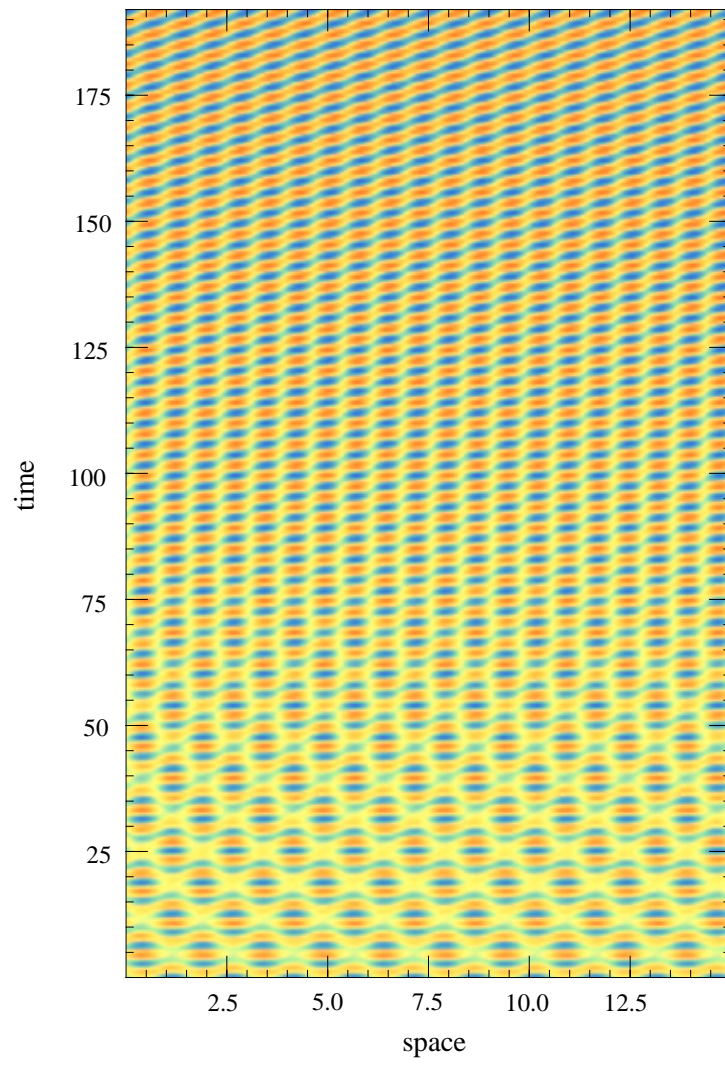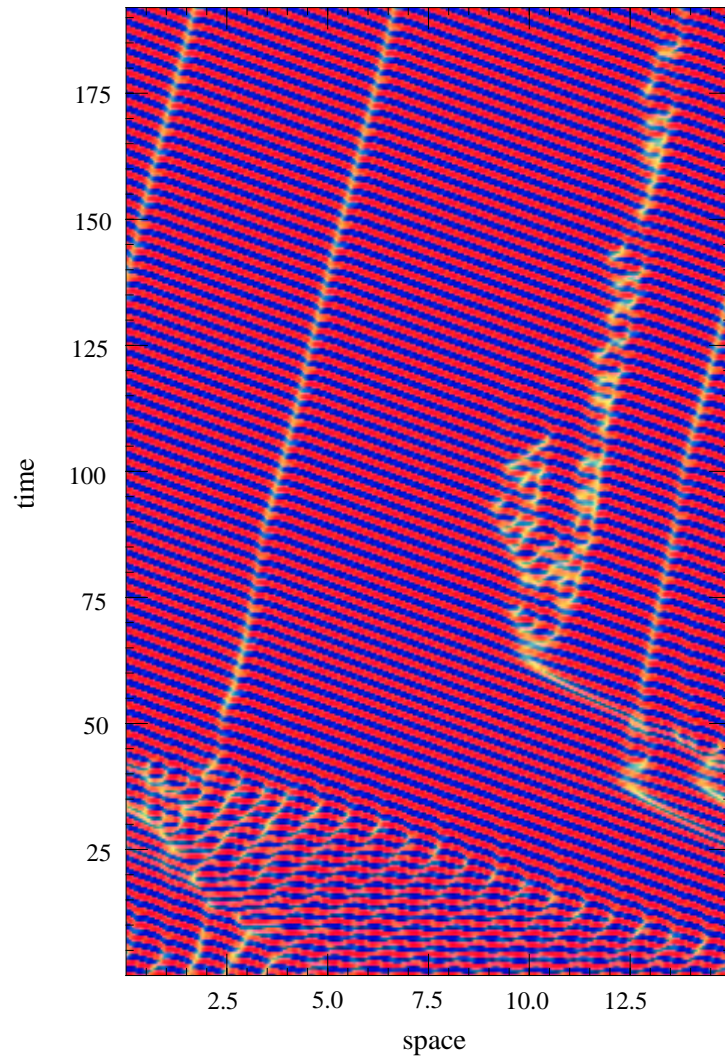
r<1

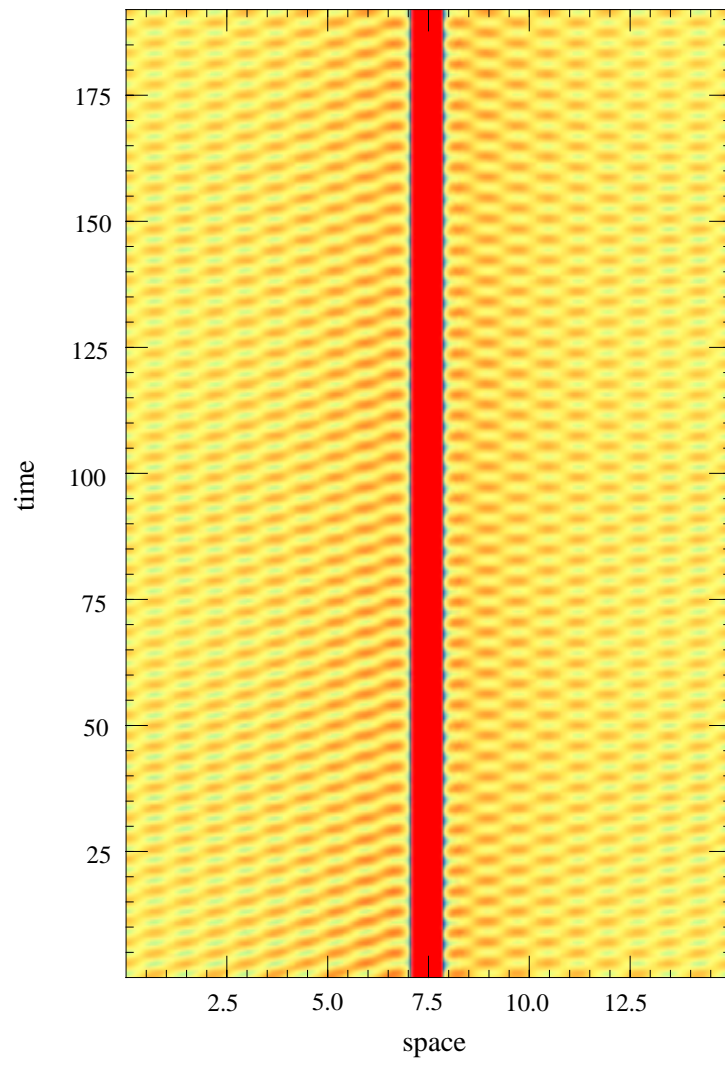r >1

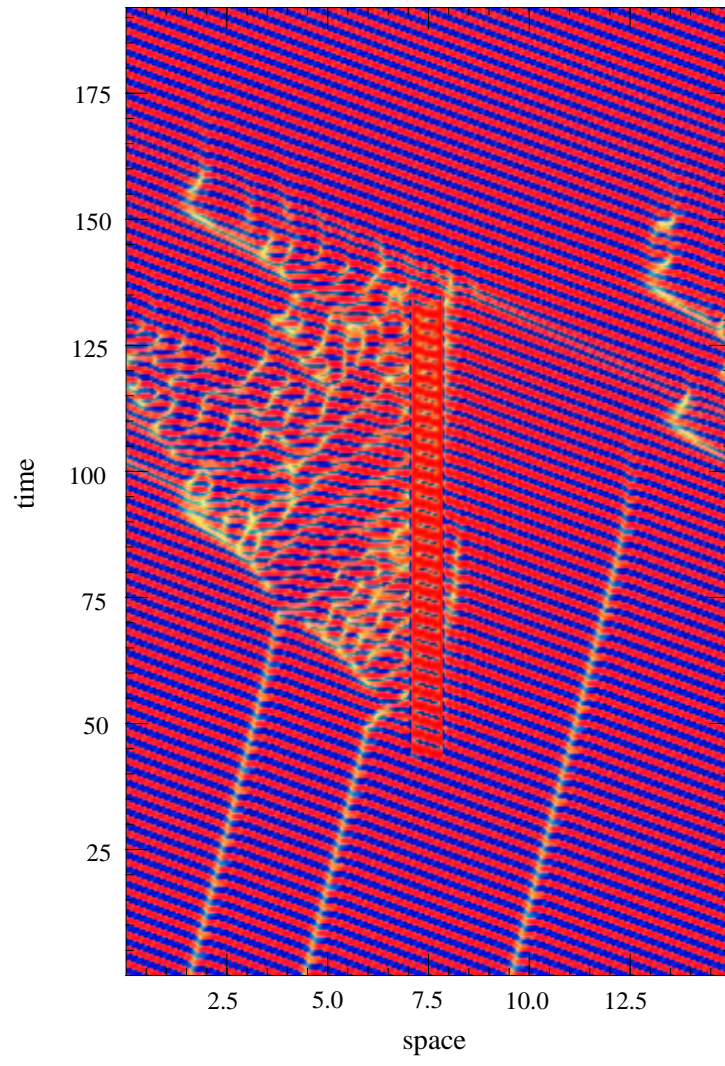|x-x'|

|x-x'|

Figure 3

21

Figure 4

Figure 5

Figure 6

Figure 7

Figure 8

Figure 9

Figure 10

Figure 11